# Large-scale Inverse Modeling of Microwave Backscatter from Sea Ice

**Quinn P. Remund and David G. Long**
**Brigham Young University, MERS Laboratory**
**459 CB, Provo, UT 84602**
**801-378-4383, FAX: 801-378-6586**
**remundq@ee.byu.edu, long@ee.byu.edu**

*Abstract*— Many forward electromagnetic scattering models have been proposed to predict the normalized radar cross section, $\sigma^o$, from sea ice characteristics. In this paper, we apply scatterometer data to large scale inverse modeling. Given the limited resolution, we adopt a simple geometric optics forward scattering model to analyze surface and volume scattering contributions to observed Ku-band signatures. A model inversion technique based on recursive optimization of an objective function is developed. Simulations demonstrate the performance of the method in the presence of noise. The inverse model is implemented using Ku-band image reconstructed data collected by the NASA scatterometer. The results are used to analyze and interpret $\sigma^o$ phenomena occurring in the Arctic.

## INTRODUCTION

Several satellite instruments have proven the utility of scatterometers in monitoring the polar regions. Among these is the NASA scatterometer (NSCAT). Ku-band NSCAT data have shown great utility in cryosphere studies [1]. NSCAT observations can be interpreted through accurate backscatter modeling. Forward scattering models have been developed to relate key surface parameters to these observed signatures. Many critical sea ice parameters are of interest to the field of cryosphere remote sensing [2]. Among these are thickness, surface roughness, salinity, snow cover, and age.

This paper describes the development and implementation of a large-scale model inversion methology based on a simple forward scattering model. The goal of the study is to provide an automated means for the inversion of microwave scattering models over vast regions rather than small individual homogeneous regions.

## BACKGROUND

Data from the NSCAT scatterometer (NSCAT) are used in the inversion study. To improve the nominal resolution of NSCAT measurements, resolution enhancement algorithms can be applied to generate images. These methods rely upon a parameterization of the dependence of $\sigma^o$ on incidence angle. Various order models can be used with increasing sensitivity to noise as order is increased. In general, $\sigma^o$ (in dB) can be modeled by

$$\sigma^\circ(dB) = A + B(\theta - 40^\circ) + C(\theta - 40^\circ)^2 + \ldots \quad (1)$$

where $\theta$ is the incidence angle, A is $\sigma^o$ normalized to 40°, B is the linear incidence angle dependence of $\sigma^o$, C is the quadratic incidence angle dependence of $\sigma^o$, and so forth.

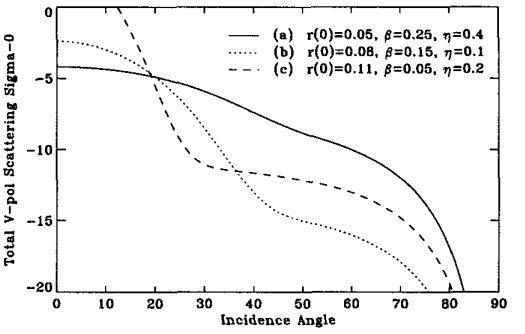


**Figure 1**: Model generated composite (volume + surface) v-pol scattering responses for sample combinations of $r(0)$, $\beta$, and $\eta$. The curves show the nonlinear nature of $\sigma^o$ as a function of incidence angle.

Several reconstruction methods can generate scatterometer imagery. For this study, polynomial coefficient images are reconstructed using the AVE algorithm [3]. The SIRF algorithm [3] can also be used, though higher order coefficients become very sensitive to noise.

A simple forward scattering model applicable to NSCAT assumes that sea ice scattering consists of incoherently summed surface and volume scattering responses [4],

$$\sigma^\circ_m = \sigma^\circ_s + \sigma^\circ_v \quad . \quad (2)$$

where $\sigma^\circ_m$ is the modeled $\sigma^o$, $\sigma^\circ_s$ is the surface scattering $\sigma^o$, and $\sigma^\circ_v$ is the volume scattering $\sigma^o$. In the interest of space, the reader is referred to [4] for a detailed description of $\sigma^\circ_s$ and $\sigma^\circ_v$. However, we note that the model is defined by three basic large-scale parameters: the nadir reflectivity, $r(0)$, the RMS surface slope $S$, and the volume scattering albedo, $\eta$. For convenience, $\beta = 2S^2$ is used in the model inversions discussed below. Figure 1 illustrates the total scattering v-pol responses for sample $r(0)$, $\beta$, and $\eta$ values.

## MODEL INVERSION METHODOLOGY

The theoretical scattering model proposed by Swift is defined by three basic parameters, $r(0)$, $\beta$, and $\eta$. These values can be estimated from observed NSCAT $\sigma^o$ signatures given sufficient incidence angle sampling. In this section, an automated inversion technique is presented for determining the three parameters from NSCAT reconstructed imagery.

The inversion approach consists of the automated steepest descent optimization of an objective function. The objective

0-7803-6359-0/00/$10.00 © 2000 IEEE

function provides a measure of the error between observed signatures and estimated model parameters,

$$J(\sigma^\circ, \vec{h}) = \sum_{\theta_i=40}^{60} [\sigma^\circ(\theta_i) - \sigma^\circ_m(\theta_i)]^2 \quad (3)$$

where $\vec{h}$ is a vector containing $[r(0), \beta, \eta]^T$. The $\sigma^\circ(\theta_i)$ response is computed given the $\sigma^o$ vs. $\theta$ variable order polynomial fit coefficients for a particular pixel in the reconstructed imagery. Hence, the optimal parameters are found at the $\vec{h}$ yielding minimum $J(\sigma^\circ, \vec{h})$.

A recursive steepest descent algorithm for computing the model parameters, and thus searching for the minimum of the objective function is given by,

$$\vec{h}(m+1) = \vec{h}(m) + \Delta(m) \odot G(m), \quad m =, 0, 1, 2, \ldots \quad (4)$$

where $\Delta$ is a vector of step sizes for each model parameter, $\odot$ is the Schur vector product, and $G(\sigma^\circ, \vec{h})$ is the steepest descent direction vector. For this study, a fixed step size is used, $\Delta = [0.001,\ 0.002,\ 0.002]^T$. The algorithm is initialized with arbitrary $\vec{h}(0)$. For a given image set of polynomial fit coefficients, the algorithm is run for each pixel. The resulting products are images of $r(0)$, $\beta$, and $\eta$.

## INVERSE MODEL SIMULATIONS

To evaluate the capability of the inversion technique, simulations are designed and implemented. "Ground truth" model parameters $r(0)$, $\beta$, and $\eta$ are forward modeled, sampled in incidence angle, and noise is added using the model, $\sigma^\circ_n(\theta_i) = \sigma^\circ(\theta_i)(1+N(0,k_p))$ where $\sigma^\circ_n(\theta_i)$ is the noise-added $\sigma^o$, $\sigma^\circ(\theta_i)$ is the original noiseless $\sigma^o$and $N(0,k_p)$ is a zero-mean Gaussian random variable. Polynomial fit coefficients are computed and used as inputs to the inverse model. For the simulations, 10 random incidence angle samples from a uniform distribution are used. Also, the simulations use $k_p$ in the range 0 to 0.1.

To offer near-comprehensive simulations which consider a broad range of ($r(0)$, $\beta$, $\eta$) combinations, synthetic "ground truth" images (shown in Figure 2) are constructed of each parameter that represent all possible sample combinations of the parameters within the ranges, $r(0) \in [0.01, 0.3]$, $\beta \in [0.05, 0.4]$, and $\eta \in [0.05, 0.4]$. The images are generated using 25 evenly spaced samples of each parameter.

The simulations are run using the 10 random incidence angle samples. Noise levels ($k_p$) are considered at 0.02 increments from 0 to 0.1. The results are summarized graphically in Figure 3. For $r(0)$ the image frames demonstrate the algorithm's ability to accurately represent the left-to-right increasing gradient as model order increases. Nearly all images show that the algorithm has difficulty in areas corresponding with very low $\beta$ values. The images also exhibit that higher order models are increasingly sensitive to noise evident as speckling in the estimate frames. For $\beta$, the first-order frames are nearly constant in value. In contrast, the second to fourth-order models

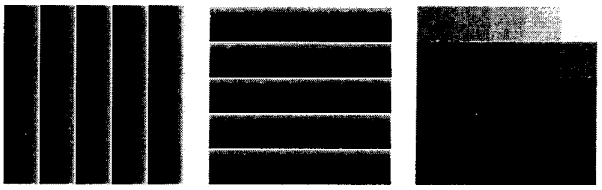

(a) $r(0)$ (b) $\beta$ (c) $\eta$

**Figure 2:** "Truth" parameter images, $r(0)$, $\beta$, and $\eta$, used in the model simulations.

are much more successful in reproducing the upward $\beta$ gradients in the truth image. Similar trends with order value exist for $\eta$ estimates as with the previous two. The first-order model has difficulty generating the constant frames in the truth image. However, all of the higher order models appear to perform relatively well.

In order to provide a quantitative measure of algorithm performance over all the possible parameter combinations, the median absolute error is used. In the interest of space, the corresponding error plots are not included. However, all of the plots indicate that parameter estimate error is lower for higher order models in the absence of noise. As $k_p$ rises, the second or third-order estimates have the lowest error. The curves also show that higher order models are increasingly sensitive to $k_p$ evident in steeper slopes in the error plots. From these results, we conclude that the second or third order $\sigma^o$ vs. $\theta$ polynomial coefficients provide the best inputs to the inverse model in the presence of noise. Since both offer similar error characteristics, the second order model will be used in the implementations with actual NSCAT data presented in the following section.

## RESULTS

The inversion method is applied to second-order NSCAT reconstructed v-pol AVE imagery ($A_v$, $B_v$, and $C_v$) to study the behavior of the technique and to interpret phenomenon observed in the reconstructed $\sigma^o$ images. A set of three Arctic AVE images representing the onset of Arctic summer is used as inverse model inputs. The ice masked image series is illustrated in Figure 4 along with model estimates discussed below. In general, multiyear ice exhibits high $A_v$ values near the centers of the images. Younger forms of ice have lower $A_v$ signatures. The phenomenon examined in this sequence is the annual drop in $\sigma^o$ observations over the ice pack.

Figure 4 also contains the image estimates of Arctic $r(0)$, $\beta$ and $\eta$. We note that the noisy values near the pole are due to insufficient incidence angle sampling caused by satellite orbit geometry and the NSCAT measurement collection configuration. The general trend in the $r(0)$ imagery consists of relatively high and low values for multiyear and first year sea ice, respectively. The melt event causes $r(0)$ to drop quickly over the entire multiyear area. Multiyear ice has typically high $\beta$ levels in contrast to lower observations over first year ice. In

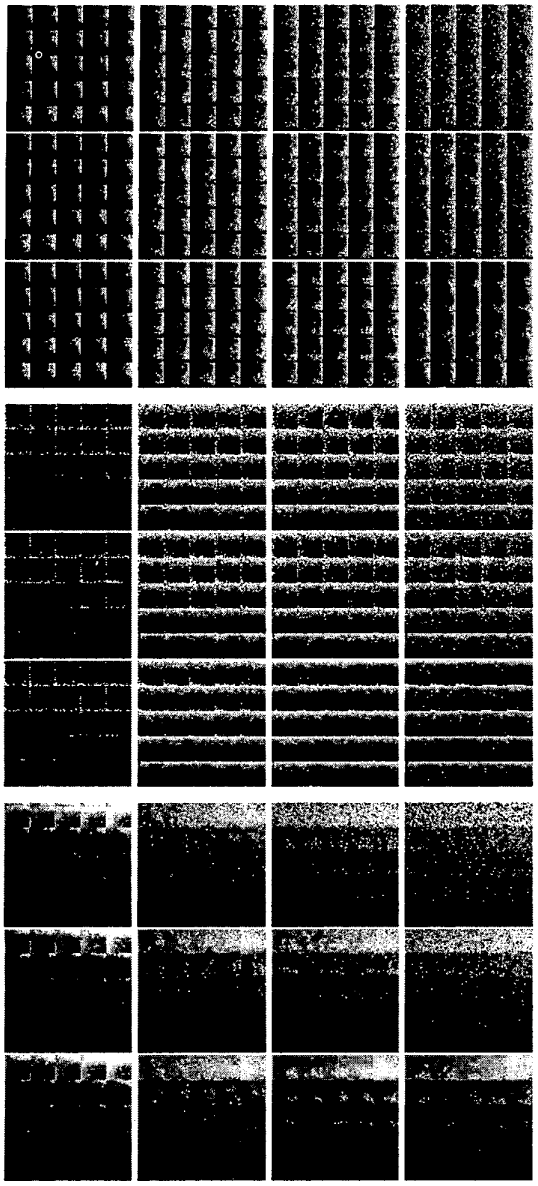

**Figure 3**: Top group: inverse model $r(0)$ parameter estimates at various $\sigma^o$ vs. $\theta$ model orders and noise levels. Middle group: $\eta$ estimates. Bottom group: $\eta$ estimates. Columns contain increasing model orders. For each group, rows contain increasing $k_p$ from 0 to .08 at .04 increments.

the second image, $\beta$ values drop until nearly the entire multiyear region appears similar to the first year $\beta$ observations. Areas of younger ice have much lower $\eta$ due to higher salinity and dielectric loss. In the last image frame, volume scattering has been almost completely masked by increased water content which reduces penetration depth.

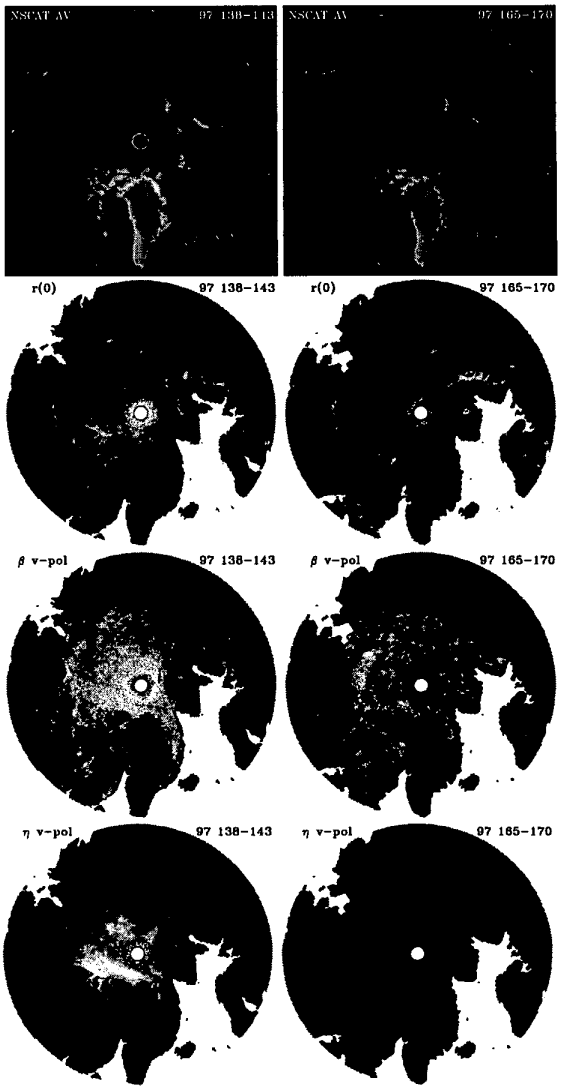


**Figure 4**: Top row: ice masked Arctic image series. Second row: inverse model estimates of $r(0) \in [0,0.1]$. Third row: estimates of $\beta \in [0.1,0.45]$. Bottom row: estimates of $\eta \in [0,0.45]$.

## REFERENCES


[1] D.G. Long and M.R. Drinkwater, "Cryosphere Applications of NSCAT Data," *IEEE Trans. on Geosci. and Rem. Sens.*, vol. 37, no. 3, pp. 1671–1684, 1999.

[2] F. Carsey, "Review and status of remote sensing of sea ice," *IEEE Journal of Oceanic Engineering*, vo. 14, pp. 127-137, 1989.

[3] D. Long, P. Hardin, and P. Whiting, "Resolution Enhancement of Spaceborne Scatterometer Data," *IEEE Trans. on Geosci. and Rem. Sens.*, vol. 31, pp. 700–715, 1993.

[4] C.T. Swift, "Seasat Scatterometer Observations of Sea Ice," *IEEE Trans. on Geosci. and Rem. Sens.*, vol. 37, no. 2, pp. 716-723, Mar. 1999.